A DISTRIBUTED LOCAL KALMAN CONSENSUS FILTER FOR TRAFFIC ESTIMATION: DESIGN, ANALYSIS AND VALIDATION

BY

YE SUN

THESIS

Submitted in partial fulfillment of the requirements
for the degree of Master of Science in Civil Engineering
in the Graduate College of the
University of Illinois at Urbana-Champaign, 2014

Urbana, Illinois

Adviser:

Professor Daniel B. Work

ABSTRACT

This thesis proposes a *distributed local Kalman consensus filter* (DLKCF) for large-scale multi-agent traffic density estimation. The *switching mode model* (SMM) describes the traffic dynamics on a stretch of roadway, and the model dynamics are linear within each mode. The error dynamics of the proposed DLKCF is shown to be *globally asymptotically stable* (GAS) when all freeway sections switch between observable modes. For an unobservable section, the estimates given by the DLKCF are proved to be ultimately bounded. We also show that under some frequently encountered conditions, the error sum in an unobservable section converges to a fixed value. Numerical experiments verify the asymptotic stability of the DLKCF for observable modes, compare the DLKCF to a Luenberger observer, illustrate the capability of the DLKCF on promoting consensus among various local agents, and show a considerable reduction of the runtime of the DLKCF compared to a central KF. Supplementary source code is available to be downloaded at https://github.com/yesun/DLKCFthesis.

ACKNOWLEDGMENTS

I would like to express my gratitude to my advisor, Professor Dan Work, who granted me access to research and life at UIUC, oriented my exploration on this interdisciplinary work, trusted my capability and potential from day one, and illustrated by example that nothing was impossible. I am greatly indebted to him for being always enthusiastic, supportive, and dedicated to perfection. He is the individual who made me believe that new ideas and solutions always exist, and I can actually be someone I could never have imagined.

I would also like to thank my parents, Fengchun Sun and Yunping Ye, for their unceasing and unconditional love and support. They gave me the cause, courage, and persistence to pursue my dream for so long, and so far away from home.

Contents

List of Tables

List of Figures

Chapter 1

Introduction

1.1 Motivation

The unprecedented growth of sensing and computational capabilities have advanced the development of real-time traffic estimation techniques. For a transportation network at the scale of a megacity, a centralized estimator that tracks the entire state of the network may require large and expensive computing resources to meet real-time constraints. An alternative is to partition large networks into local regions, with each region estimated by a cheap commodity computer (e.g. an agent), thus easing the computational burden. However, without coordination between adjacent or overlapping partitions, estimates provided by different agents may disagree on the estimates on the shared boundaries. This motivates the introduction of information sharing among agents to compensate for the lack of a central estimator, thus enhancing estimation consistency while also enabling computational scalability.

1.2 Related work

A number of sequential state estimation algorithms have been proposed to estimate traffic conditions. The *Switching Mode Model* (SMM) (Sun et al., 2003, 2004; Munoz et al., 2006) is a piecewise linear form of the *Cell Transmission Model* (CTM)

(Daganzo, 1994, 1995; Lebacque, 1996), and is integrated into the *Mixture Kalman Filter* in Sun et al. (2004) for ramp metering. A proof of the stability and a derivation of an error conservation property of a Luenberger observer based on the SMM is provided in Morarescu and Canudas de Wit (2011), which serves as an inspiration for this work and is extended in Canudas de Wit et al. (2012) for more accurate mode estimation. In Thai and Bayen (2013), the *Interacting Multiple Model* algorithm is applied to the SMM with generalized modes. A robust mode selector is proposed in Morbidi et al. (2014) to determine the most probable mode of the uncertain graph-constrained SMM. A Gaussian approximation of the stochastic traffic model Jabari and Liu (2012) is solved by the standard *Kalman Filter* (KF) in Jabari and Liu (2013), which shows the stochastic observability of the proposed model by the boundedness of covariance matrices. The *Parallelized Particle Filters* and the *Parallelized Gaussian Sum Particle Filter* are designed in Mihaylova et al. (2012) for computational scalability. Other treatments of traffic estimation include Wang and Papageorgiou (2005); Mihaylova et al. (2007); Work et al. (2010); Chen and Rakha (2012); Yuan et al. (2012). A recent overview of sequential estimation techniques for scalar traffic models can be found in Blandin et al. (2012).

Research on collaborative information processing is driven by the broad applications of multi-agent systems (Lynch, 1997; Fax and Murray, 2004; Santoro, 2007; Mesbahi and Egerstedt, 2010). The *decentralized Kalman filter* (Speyer, 1979; Rao et al., 1993) requires a complete communication network with all-to-all links which may not scale in large-scale systems. A scalable *Distributed Kalman Filter* (DKF) is introduced in Olfati-Saber (2005), and the work of Khan and Moura (2008) partitions the large-scale systems into subsystems to reduce computation load, with observation fusion applied on the shared states between subsystems to ensure consensus. In the *Kalman-Consensus Filter* (KCF), consensus is achieved by communication on the state estimates (Olfati-Saber, 2007). A formal analysis on the

stability of the KCF can be found in Olfati-Saber (2007) for continuous systems, and in Olfati-Saber (2009) for discrete-time systems.

1.3 Contributions and outline of the thesis

The main contribution of this thesis is the design and analysis of a *Distributed Local Kalman Consensus Filter* (DLKCF) to estimate the traffic density on freeways, with system dynamics chosen to be the SMM. The transportation network is partitioned into local regions (sections) with overlapping areas on the boundaries. Each agent provides a *local* estimate on its own region, and shares sensor data and state estimates with its adjacent overlapping *neighbors*. Furthermore, *consensus* on the overlapping areas is pursued to achieve agreement on the estimates of the common state shared between neighbors. We provide a formal proof of the stability and boundedness of the DLKCF under various observability scenarios, which has been missing from many traffic estimation methods.

This work is organized as follows. Chapter 2 summarizes the CTM and the SMM, and Chapter 3 introduces the DLKCF. In Section 4.1, we prove that the DLKCF is globally asymptotically stable under the observable modes of the SMM. For an unobservable section, we prove in Section 4.2.1 that the state estimates are ultimately bounded, and Section 5.2 proves the convergence of the sum of the state errors. Finally, numerical experiments are presented in Chapter 5, which verify the proved results, and show the advantage of the DLKCF on promoting consensus on the estimates between neighbors, reducing the estimation error under low quality sensing/estimating units, as well as easing the computation load for each local agent.

Chapter 2

Scalar macroscopic traffic modeling

Macroscopic traffic modeling considers traffic flowing dynamics as a continuum of vehicles, rather than modeling behaviors of individual vehicles on a stretch of roadway. Macroscopic traffic models are originally motivated by constitutive hydrodynamics models, where the fluid dynamics resembles properties of traffic flow. Scalar traffic models classically consider the traffic state at a point x at time t to be fully represented by the vehicle density $\rho(t, x)$, as opposed to non-scalar models which also include additional state variables such as vehicle velocity, etc., to take into account additional physical principles. To simplify the analysis, the discretized link models describe the vehicle densities on a discretization grid of the spacial-temporal domain. This chapter introduces CTM, one of the most common scalar discretized link traffic models, as well as its piecewise linear form–SMM–which is later integrated into our traffic estimation problem. Since this thesis studies traffic estimation based on a scalar model, we omit details on non-scalar models and the reader is referred to Payne (1971) and Whitham (1974) for more involved readings.

2.1 Cell transmission model

The classical scalar model describing the evolution of traffic density $\rho(t, x)$ on a road network at location x and time t is the *Lighthill-Whitham-Richards* (LWR) *Partial Differential Equation* (PDE) (Richards, 1956; Lighthill and Whitham, 1955), which describes vehicle conservation:

$$\partial_t \rho + \partial_x Q(\rho) = 0. \tag{2.1}$$

The function $Q(\rho) = \rho v(\rho)$ is called the flux function, where $v(\rho)$ is an empirical velocity function used to close the model. The triangular flux function (Daganzo, 1995) used in this work is given by

$$Q(\rho) = \begin{cases} \rho v_m & \text{if } \rho \in [0, \rho_c] \\ \rho_c v_m \frac{\rho_m - \rho}{\rho_m - \rho_c} & \text{if } \rho \in [\rho_c, \rho_m], \end{cases} \tag{2.2}$$

where v_m denotes the *freeflow speed* and ρ_m denotes the *maximum density*. The variable ρ_c is the *critical density* at which the maximum flux is realized. For the triangular fundamental diagram, the flux function has different slopes in *freeflow* ($\rho \leq \rho_c$) and *congestion* ($\rho > \rho_c$). In freeflow, the slope is v_m, and in congestion, it is $w = \frac{\rho_c v_m}{\rho_m - \rho_c}$.

The CTM is a discretization of (2.1) and (2.2) using a *Godunov scheme* (Godunov, 1959). Consider a discretization grid defined by a space step Δx and a time step Δt. We let l index the cell defined by $x \in [l\Delta x, (l+1)\Delta x)$, and denote by ρ_k^l the density at time $k\Delta t$ in cell l. The discretized version of the model described in (2.1) becomes

$$\rho_{k+1}^l = \rho_k^l + \frac{\Delta t}{\Delta x} \left(q(\rho_k^{l-1}, \rho_k^l) - q(\rho_k^l, \rho_k^{l+1}) \right), \tag{2.3}$$

where $q(\rho_k^{l-1}, \rho_k^l)$ is the flux between cell $l-1$ and l, which is determined by:

$$q(\rho_k^{l-1}, \rho_k^l) = \min\{v_m \rho_k^{l-1}, w(\rho_m - \rho_k^l), q_m\}, \tag{2.4}$$

where q_m is the maximum flow given by $q_m = v_m \rho_c$.

2.2 Switching mode model

In the SMM, the discretized LWR PDE (2.3) is written as a hybrid system whose evolution equation switches among different linear modes, depending on the state of the upstream and downstream cells.

2.2.1 Definition of modes and evolution equations

Consider discretizing a freeway section into n cells, and define the state vector of the section to be $\rho_k = (\rho_k^1, \cdots, \rho_k^n)^T$. We make the following three assumptions for traffic estimation with the SMM:

1. the densities of the upstream and downstream cells in each section are measured, since freeway sections are usually partitioned at locations with sensors;

2. there is at most one transition between freeflow and congestion within each section, which is motivated by the fact that freeway sections are generally short with no more than one queue building up or dissipating; and

3. the boundary density measurements are sufficiently accurate to distinguish between four of the five modes described next, but they cannot determine the location or direction of the shock (some comments on this assumption follow on Chapter 3 below).

Given the second assumption above, a road section may switch between the following five modes:

1. *freeflow–freeflow* (FF), in which all cells in the section are in freeflow;

2. *congestion–congestion* (CC), in which all cells in the section are in congestion;

3. *congestion–freeflow* (CF), in which the cells in the upstream part of the section are congested, and the cells in the downstream part are in freeflow;

4. *freeflow–congestion 1* (FC1), in which the upstream part of the section is in freeflow, the downstream part is in congestion, and the shock has positive velocity or is stationary; and

5. *freeflow–congestion 2* (FC2), in which the upstream part of the section is in freeflow, the downstream part is in congestion, and the shock has negative velocity.

Note the boundary sensors cannot distinguish between modes 4 and 5. In each mode stated above, the traffic state ρ_k evolves with linear dynamics, forming a hybrid system:

$$\rho_{k+1} = A_{\sigma(k),s(k)}\rho_k + B^{\rho}_{\sigma(k),s(k)}\boldsymbol{\rho}_m + B^{q}_{\sigma(k),s(k)}\boldsymbol{q}_m, \tag{2.5}$$

where $\boldsymbol{\rho}_m = (\rho_m, \cdots, \rho_m)^T \in \mathbb{R}^n$, $\boldsymbol{q}_m = (q_m, \cdots, q_m)^T \in \mathbb{R}^n$, and $A_{\sigma(k),s(k)}$, $B^{\rho}_{\sigma(k),s(k)}$, $B^{q}_{\sigma(k),s(k)} \in \mathbb{R}^{n\times n}$ are matrices to be defined precisely later. The mode index $\sigma(k) \in \mathcal{S}$ where $\mathcal{S} = \{1, 2, 3, 4, 5\}$ is the index set denoting the five modes, and $s(k) \in \{0, 1, \cdots, n\}$ is the index introduced to precisely locate the transition between freeflow and congestion when it exists. We say $s(k) = l$ when the transition occurs between cell l and $l + 1$.

To explicitly define (2.5) in each mode, some notation is introduced. For all $p \in \{1, 2, \cdots, n-1\}$, define $\Gamma_p \in \mathbb{R}^{p\times p}$ and $\Delta_p \in \mathbb{R}^{p\times p}$ by their $(i,j)^{\text{th}}$ entries as

$$\Gamma_p(i,j) = \begin{cases} 1 - \frac{v_m\Delta t}{\Delta x} & \text{if } i = j \\ \frac{v_m\Delta t}{\Delta x} & \text{if } i = j+1 \\ 0 & \text{otherwise,} \end{cases}$$

$$\Delta_p(i,j) = \begin{cases} 1 - \frac{w\Delta t}{\Delta x} & \text{if } i = j \\ \frac{w\Delta t}{\Delta x} & \text{if } i = j-1 \\ 0 & \text{otherwise.} \end{cases}$$

In the FF mode, the mode index $\sigma = 1$, and $s(k) = 0$. The explicit forms of $A_{\sigma,s}$, $B^{\rho}_{\sigma,s}$, and $B^{q}_{\sigma,s}$ are:

$$A_{1,0} = \begin{pmatrix} 1 & \mathbf{0}_{1,n-1} \\ \begin{pmatrix} \frac{v_m \Delta t}{\Delta x} \\ \mathbf{0}_{n-2,1} \end{pmatrix} & \Gamma_{n-1} \end{pmatrix}, B^{\rho}_{1,0} = B^{q}_{1,0} = \mathbf{0}.$$

where $\mathbf{0}_{i,j} \in \mathbb{R}^{i \times j}$ which is zero everywhere, and $\mathbf{0} = \mathbf{0}_{n,n}$.

In the CC mode, the mode index $\sigma = 2$, and $s(k) = n$. The explicit forms of $A_{\sigma,s}$, $B^{\rho}_{\sigma,s}$, and $B^{q}_{\sigma,s}$ are:

$$A_{2,n} = \begin{pmatrix} \Delta_{n-1} & \begin{pmatrix} \mathbf{0}_{n-2,1} \\ \frac{w \Delta t}{\Delta x} \end{pmatrix} \\ \mathbf{0}_{1,n-1} & 1 \end{pmatrix}, B^{\rho}_{2,n} = B^{q}_{2,n} = \mathbf{0}.$$

In the CF mode, the mode index $\sigma = 3$, and the explicit forms of $A_{\sigma,s}$, $B^{\rho}_{\sigma,s}$, and $B^{q}_{\sigma,s}$ are:

$$A_{3,s} = \begin{pmatrix} \Delta_s & \mathbf{0}_{s,n-s} \\ \mathbf{0}_{n-s,s} & \Gamma_{n-s} \end{pmatrix}, B^{\rho}_{3,s} = \mathbf{0} + \frac{w \Delta t}{\Delta x} E_{s,s},$$

$$B^{q}_{3,s} = \mathbf{0} - \frac{\Delta t}{\Delta x} E_{s,s+1} + \frac{\Delta t}{\Delta x} E_{s+1,s+1},$$

where $E_{i,j}$ are matrices that are zero everywhere but the $(i,j)^{\text{th}}$ entry, which is one. Note that s may take any value in $\{1, \cdots, n-1\}$, depending on the location of the center of the expansion fan connecting the congested and freeflow states.

In the two FC modes, define $\hat{\Gamma}_p$ and $\hat{\Delta}_p$ as follows:

$$\hat{\Gamma}_p = \begin{cases} \begin{pmatrix} 1 & \mathbf{0}_{1,p} \\ \begin{pmatrix} \frac{v_m \Delta t}{\Delta x} \\ \mathbf{0}_{p-1,1} \end{pmatrix} & \Gamma_p \end{pmatrix} & \text{if } p \in \{1, \cdots, n-1\}, \\ 1 & \text{if } p = 0, \end{cases}$$

and

$$\hat{\Delta}_p = \begin{cases} \begin{pmatrix} \Delta_p & \begin{pmatrix} \mathbf{0}_{1,p-1} \\ \frac{w\Delta t}{\Delta x} \end{pmatrix} \\ \mathbf{0}_{1,p} & 1 \end{pmatrix} & \text{if } p \in \{1, \cdots, n-1\}, \\ 1 & \text{if } p = 0. \end{cases}$$

When $\sigma = 4$ and $s \in \{1, \cdots, n-2\}$, or $\sigma = 5$ and $s \in \{2, \cdots, n-1\}$, the explicit forms of $A_{\sigma,s}$, $B^{\rho}_{\sigma,s}$, and $B^{q}_{\sigma,s}$ are:

$$A_{\sigma,s} = \begin{pmatrix} \hat{\Gamma}_{\tilde{s}-1} & \mathbf{0}_{\tilde{s},1} & \mathbf{0}_{\tilde{s},\bar{s}} \\ \begin{pmatrix} \mathbf{0}_{1,\tilde{s}-1} & \frac{v_m \Delta t}{\Delta x} \end{pmatrix} & 1 & \begin{pmatrix} \frac{w\Delta t}{\Delta x} & \mathbf{0}_{1,\bar{s}-1} \end{pmatrix} \\ \mathbf{0}_{\bar{s},\tilde{s}} & \mathbf{0}_{\bar{s},1} & \hat{\Delta}_{\bar{s}-1} \end{pmatrix},$$

$$B^{\rho}_{\sigma,s} = \begin{pmatrix} \mathbf{0}_{\tilde{s}+1,\tilde{s}+1} & \begin{pmatrix} \mathbf{0}_{\tilde{s},1} & \mathbf{0}_{\tilde{s},\bar{s}-1} \\ -\frac{w\Delta t}{\Delta x} & \mathbf{0}_{1,\bar{s}-1} \end{pmatrix} \\ \mathbf{0}_{\bar{s},\tilde{s}+1} & \mathbf{0}_{\bar{s},\bar{s}} \end{pmatrix}, B^{q}_{\sigma,s} = \mathbf{0},$$

where for $\sigma = 4$ we have $\tilde{s} = s$ and $\bar{s} = n - s - 1$, and for $\sigma = 5$ we have $\tilde{s} = s - 1$ and $\bar{s} = n - s$.

When $\sigma = 4$ and $s = n - 1$, we have $A_{\sigma,s} = \text{diag}\left(\hat{\Gamma}_{n-2}, 1\right)$ (i.e. with $\hat{\Gamma}_{n-2}$ and 1 on the diagonal) , and $A_{\sigma,s} = \text{diag}\left(1, \hat{\Delta}_{n-2}\right)$ when $\sigma = 5$ and $s = 1$. For both cases, we have $B^{\rho}_{\sigma,s} = B^{q}_{\sigma,s} = \mathbf{0}$.

2.2.2 Observability

The observability results of the SMM for individual modes are summarized in Table 2.1 (Munoz et al., 2006). It can be derived directly from standard linear system techniques for each mode given the system model (2.5) and the observation equation

$$z_k = H_k \rho_k, \tag{2.6}$$

where z_k is the measurement vector, and H_k is the appropriate output matrix.

Table 2.1: Observability of the SMM[1,2] (Munoz et al., 2006)

Mode	U	D	Shock velocity	Observable with
1	F	F	no shock	D measurement
2	C	C	no shock	U measurement
3	C	F	no shock	U and D measurements
4	F	C	positive or stationary	unobservable
5	F	C	negative	unobservable

[1] F and C represent freeflow and congested, respectively.
[2] U and D represent upstream and downstream, respectively.

Remark 1. *In the SMM proposed in Sun et al. (2003); Munoz et al. (2006), an additional assumption requires the precise inflow and outflow of the section as inputs of the system. Here we instead assign constant dynamics for the boundary cells subject to some uncertainty. It is assumed that boundary measurements will be available and will be integrated through the update equation within the filter. As a result the system dynamics no longer depends on cell densities outside the section, at the expense of a correct model at the boundary. This treatment is made since: (i) measurements of boundary conditions cannot be treated as the true input of the system without accounting for measurement errors, and (ii) for distributed computational platforms, independence of system dynamics for each section is desirable. Note that all results and proofs in this work hold for either formulation.*

Chapter 3

Distributed local Kalman consensus filter

Given a dynamic system with a collection of state measurements up to the current time, the *filtering problem* aims at computing the *optimal estimate* of the current state. This consists of iteratively updating the state estimate once a new measurement becomes available, yielding a so-called *sequential* estimation scheme. The KF is one of the most well-known sequential estimation algorithm which relies on the *Bayes' rule* to compute the conditional distribution of the state given the available measurements, and the *minimum mean square error* (MMSE) optimality criterion to obtain the optimal estimate. In this chapter, we review the KF and provide an explicit expression of the proposed DLKCF.

3.1 Kalman filter

In this section, we briefly review the KF and introduce notation needed later in the proposed filter. Consider a linear time-varying model

$$\rho_{k+1} = A_k \rho_k + w_k,\ \rho_k \in \mathbb{R}^n, \tag{3.1}$$

where $w_k \sim \mathcal{N}(0, Q_k)$. Sensor measurements z_k are modeled by the following linear observation equation

$$z_k = H_k \rho_k + v_k,\ z_k \in \mathbb{R}^m, \tag{3.2}$$

where H_k and $v_k \sim \mathcal{N}(0, R_k)$ are the observation matrix and measurement noise, respectively.

Given the sensor data up to time k denoted by $Z_k = \{z_0, \cdots, z_k\}$, the *prior estimate* and *posterior estimate* of the state can be expressed as $\rho_{k|k-1} = E[\rho_k | Z_{k-1}]$ and $\rho_{k|k} = E[\rho_k | Z_k]$, respectively. Let $\eta_{k|k-1} = \rho_{k|k-1} - \rho_k$ and $\eta_{k|k} = \rho_{k|k} - \rho_k$ denote the prior and posterior estimation errors. The state error covariance matrices associated with $\rho_{k|k-1}$ and $\rho_{k|k}$ are given by $\Gamma_{k|k-1} = E[\eta_{k|k-1}\eta_{k|k-1}^T | Z_{k-1}]$ and $\Gamma_{k|k} = E[\eta_{k|k}\eta_{k|k}^T | Z_k]$. The KF sequentially computes $\rho_{k|k}$ from $\rho_{k-1|k-1}$ as follows:

$$\text{Forecast:} \begin{cases} \rho_{k|k-1} = A_{k-1}\rho_{k-1|k-1} \\ \Gamma_{k|k-1} = A_{k-1}\Gamma_{k-1|k-1}A_{k-1}^T + Q_{k-1}, \end{cases}$$

$$\text{Analysis:} \begin{cases} \rho_{k|k} = \rho_{k|k-1} + K_k(z_k - H_k\rho_{k|k-1}) \\ \Gamma_{k|k} = \Gamma_{k|k-1} - K_k H_k \Gamma_{k|k-1} \\ K_k = \Gamma_{k|k-1}H_k^T(R_k + H_k\Gamma_{k|k-1}H_k^T)^{-1}, \end{cases}$$

where K_k is the *Kalman gain*, and $z_k - H_k\rho_{k|k-1}$ is the *innovation*. In the KF, the forecast step updates the mean and error covariance of the estimate through the system model given in (3.1), and the analysis step refines the estimate based on the latest obtained measurements.

3.2 Distributed local Kalman consensus filter

The DLKCF is a localized version of the KCF, which itself is an extension of the KF for multi-agent estimation (Olfati-Saber, 2007, 2009). Consider a network with an ad hoc undirected communication topology between agents given by the graph

$\mathcal{G} = (\mathcal{V}, \mathcal{E})$, where $\mathcal{V}$ and $\mathcal{E}$ are the vertex and edge sets, respectively. For agent i the output equation is given by

$$z_{i,k}^{\mathrm{d}} = H_{i,k}^{\mathrm{d}} \rho_k + v_{i,k}^{\mathrm{d}},\ z_{i,k}^{\mathrm{d}} \in \mathbb{R}^{m_i},$$

where the superscript d stands for distributed, and $v_{i,k}^{\mathrm{d}} \sim \mathcal{N}\left(0, R_{i,k}^{\mathrm{d}}\right)$. Let $\mathcal{N}_i = \{j : (i,j) \in \mathcal{E}\}$ be the set of neighboring agents of agent i on graph $\mathcal{G}$, and define $\mathcal{J}_i = \mathcal{N}_i \bigcup \{i\}$. In the KCF, through communication each agent possesses columnized measurement vector $z_{i,k} = \mathrm{col}_{j \in \mathcal{J}_i}\left(z_{j,k}^{\mathrm{d}}\right)$ and a corresponding columnized output matrix $H_{i,k} = \mathrm{col}_{j \in \mathcal{J}_i}\left(H_{j,k}^{\mathrm{d}}\right)$, as well as a block diagonal measurement error covariance matrix $R_{i,k} = \mathrm{diag}_{j \in \mathcal{J}_i}\left(R_{j,k}^{\mathrm{d}}\right)$. A consensus term is computed based on the disparities of the prior estimates among neighbors and is applied to the analysis step to promote agreement on estimates among neighboring agents.

For the KCF stated above, each agent estimates all the state variables of ρ_k. However, for estimation on large-scale transportation systems, this is neither computationally efficient nor practically necessary. Consequently, a localized version of the KCF, namely the DLKCF, is introduced. The DLKCF partitions the state into local overlapping subsets, and each agent estimates a single subset of the state.

The freeway network is partitioned into N local sections, with overlapping regions established to allow communication between neighboring agents to exchange messages on measurements and state estimates. From the SMM in section 2.2, the system dynamics of the i^{th} section is given by

$$\rho_{i,k+1} = A_{i,k}\rho_k + B_{i,k}^{\rho}\boldsymbol{\rho}_m + B_{i,k}^{q}\boldsymbol{q}_m, \rho_{i,k} \in \mathbb{R}^{n_i}. \tag{3.3}$$

Note that in (3.3) and for the remainder of the thesis the subscripts for A, B^{ρ}, and B^{q} are slightly different from what was used in (2.5) with $\sigma(k)$ and $s(k)$. Since both $\sigma(k)$ and $s(k)$ are dependent on k, we let subscript k combine their effects, and add an subscript $i \in \mathcal{I} = \{1, 2, \cdots, N\}$ to denote the section index. We denote the dimension of the overlapping region between section i and section j as $n_{i,j}$. For the

freeway network, the neighborhood of section i is defined as

$$\mathcal{N}_i = \begin{cases} \{i+1\} & \text{if } i = 1 \\ \{i-1, i+1\} & \text{if } i \neq 1, \text{ and } i \neq N \\ \{i-1\} & \text{if } i = N. \end{cases}$$

For $j \in \mathcal{N}_i$, define matrix operator $\hat{I}_{i,j}$ as

$$\hat{I}_{i,j} = \begin{cases} \begin{pmatrix} I_{n_{i,j}} & \mathbf{0}_{n_{i,j}, n_i - n_{i,j}} \end{pmatrix} & \text{if } j = i-1 \\ \begin{pmatrix} \mathbf{0}_{n_{i,j}, n_i - n_{i,j}} & I_{n_{i,j}} \end{pmatrix} & \text{if } j = i+1, \end{cases} \tag{3.4}$$

where $I_{n_{i,j}} \in \mathbb{R}^{n_{i,j}}$ is the identity matrix, and the operation $\hat{I}_{i,j}\rho_{i,k}$ selects the part of agent i's state that overlaps with agent j.

Formally the forecast and analysis steps of the DLKCF for the i^{th} agent are written as

$$\begin{cases} \rho_{i,k|k-1} = A_{i,k-1}\rho_{i,k-1|k-1} \\ \Gamma_{i,k|k-1} = A_{i,k-1}\Gamma_{i,k-1|k-1}A_{i,k-1}^T + Q_{i,k-1}, \end{cases} \tag{3.5}$$

$$\begin{cases} \rho_{i,k|k} &= \rho_{i,k|k-1} + K_{i,k}\left(z_{i,k} - H_{i,k}\rho_{i,k|k-1}\right) \\ &\quad + \sum_{j\in\mathcal{N}_i} C_{i,k}^j \left(\hat{I}_{j,i}\rho_{j,k|k-1} - \hat{I}_{i,j}\rho_{i,k|k-1}\right) \\ \Gamma_{i,k|k} &= \Gamma_{i,k|k-1} - K_{i,k}H_{i,k}\Gamma_{i,k|k-1} \\ K_{i,k} &= \Gamma_{i,k|k-1}H_{i,k}^T(R_{i,k} + H_{i,k}\Gamma_{i,k|k-1}H_{i,k}^T)^{-1}, \end{cases} \tag{3.6}$$

where $C_{i,k}^j$ is the *consensus gain* of agent i associated with neighbor j at time step k, and for simplicity we drop the last two terms in (3.3) independent of the state. Our choice for the consensus gain for the observable modes is inspired by the work of Olfati-Saber (2009), and the consensus term is dropped for the unobservable modes. Hence the choice of the consensus gain reads:

$$C_{i,k}^j = \begin{cases} \gamma_{k-1}F_{i,k}G_{i,k}\hat{I}_{i,j}^T & \sigma(k) \in \{1,2,3\} \\ \mathbf{0} & \sigma(k) \in \{4,5\}, \end{cases} \tag{3.7}$$

where

$$\begin{aligned} F_{i,k} =& I - K_{i,k}H_{i,k}, \\ G_{i,k} =& A_{i,k-1}\Gamma_{i,k-1|k-1}A_{i,k-1}^T + Q_{i,k-1} \\ &+ \Gamma_{i,k|k-1}S_{i,k}\Gamma_{i,k|k-1}, \end{aligned} \tag{3.8}$$

where $S_{i,k} = H_{i,k}^T R_{i,k}^{-1} H_{i,k}$ is the *information matrix*, and γ_k is a sufficiently small scaling factor, whose explicit form will be given in Chapter 4 to ensure stability of the filter.

Remark 2. *The assumption in* (3.1) *that* $w_k \sim \mathcal{N}(0, Q_k)$*, independent of* ρ_k*, results in an approximation to the real traffic model, whose side effect would be enlarged with an inaccurate estimate of the model (i.e. the matrix* $A_{i,k}$*). In the DLKCF, based on assumption (*iii*) of the SMM, the matrix* $A_{i,k}$ *can ultimately be correctly reconstructed by the local agent in observable modes. For unobservable modes, the agent needs to apply an estimate* $\hat{A}_{i,k}$ *of* $A_{i,k}$ *based on state estimate* $\rho_{i,k|k}$ *to run the filter. When assumption (*iii*) of the SMM is released, the performance of the filter would be improved under a constrained-CTM (Canudas de Wit et al., 2012) which aims at reducing the estimation error due to the measurement and model uncertainties.*

Chapter 4

Stability of the DLKCF for traffic estimation

In this chapter, we show that for a network where all sections switch among observable modes, the error dynamics is *globally asymptotically stable* (GAS). For an unobservable section, we show that despite the lack of knowledge on the precise form of the state equations due to the unknown shock location and direction, the estimate of the state is physically meaningful. Furthermore, under some frequently satisfied conditions specified later, the one-step change in the estimated total number of vehicles in the unobservable section converges to the true one-step change.

4.1 Asymptotic stability of error dynamics in observable modes

We define the prior and posterior estimation errors for section i as $\eta_{i,k|k-1} = \rho_{i,k|k-1} - \rho_{i,k}$ and $\eta_{i,k|k} = \rho_{i,k|k} - \rho_{i,k}$, and define the neighbor disagreement as

$$u_{i,k}^{j} = \hat{I}_{j,i}\eta_{j,k|k-1} - \hat{I}_{i,j}\eta_{i,k|k-1}. \tag{4.1}$$

The global estimation error $\eta_{k|k}$ is reconstructed by $\eta_{k|k} = \mathrm{col}(\eta_{1,k|k}, \cdots, \eta_{N,k|k})$, and the estimation error in section i evolves as follows (without model and measurement

noise):

$$\eta_{i,k|k} = F_{i,k} A_{i,k-1} \eta_{i,k-1|k-1} + \sum_{j \in \mathcal{N}_i} C^j_{i,k} u^j_{i,k}. \tag{4.2}$$

We consider the following *common Lyapunov function* candidate which reads:

$$V(k, \eta_{k|k}) = \sum_{i=1}^{N} \eta^T_{i,k|k} \Gamma^{-1}_{i,k|k} \eta_{i,k|k}, \tag{4.3}$$

and compute its one-step change $\delta V(k, \eta_{k|k})$ by applying (4.2) as follows:

$$\begin{aligned} \delta V(k, \eta_{k|k}) &= V(k+1, \eta_{k+1|k+1}) - V(k, \eta_{k|k}) \\ &= \textstyle\sum_{i=1}^{N} \eta^T_{i,k|k} \left(A^T_{i,k} F^T_{i,k+1} \Gamma^{-1}_{i,k+1|k+1} F_{i,k+1} A_{i,k} - \Gamma^{-1}_{i,k|k} \right) \eta_{i,k|k} \\ &\quad + 2 \textstyle\sum_{i=1}^{N} \left(\eta^T_{i,k+1|k} F^T_{i,k+1} \Gamma^{-1}_{i,k+1|k+1} \sum_{j \in \mathcal{N}_i} C^j_{i,k+1} u^j_{i,k+1} \right) \\ &\quad + \textstyle\sum_{i=1}^{N} \left(\sum_{j \in \mathcal{N}_i} C^j_{i,k+1} u^j_{i,k+1} \right)^T \Gamma^{-1}_{i,k+1|k+1} \left(\sum_{j \in \mathcal{N}_i} C^j_{i,k+1} u^j_{i,k+1} \right). \end{aligned} \tag{4.4}$$

To ensure the asymptotic stability of the error dynamics holds globally, the common Lyapunov function (4.3) needs to be *radically unbounded*[1], which means that the error covariance matrix $\Gamma_{i,k|k}$ needs to be upper bounded for all i and k. This holds by the following lemma.

Lemma 1 (Boundedness of the estimation error covariance matrix in the KF for an arbitrary switching sequence in observable modes (Boker and Lunze, 2002))**.** *If the hybrid system* (3.3) *switches among observable modes for all i and k, the error covariance matrix $\Gamma_{i,k|k}$ given in* (3.6) *is upper bounded for all i and k, independent of the switching sequence.*

The next lemma provides a result on the Laplacian of an undirected graph, which is important for treatment of the consensus term in the stability proof of the DLKCF.

[1]Recall that a function $V(\cdot, \eta)$ is radically unbounded if it satisfies $V(\cdot, \eta) \to \infty$ as $\|\eta\| \to \infty$

Lemma 2 (Quadratic property of the Laplacian of an undirected graph (Godsil and Royle, 2001; Olfati-Saber et al., 2007)). *The following holds for the n-dimensional Laplacian $\bar{L}$ of any undirected graph $\mathcal{G} = (\mathcal{V}, \mathcal{E})$ with N vertices, irrespective of its connectivity:*

$$\sum_{i=1}^{N} \sum_{j \in \mathcal{N}_i} \xi_i(\xi_j - \xi_i) = -\frac{1}{2} \sum_{(i,j) \in \mathcal{E}} \|\xi_j - \xi_i\|^2 = -\xi^T \bar{L} \xi,$$

where $\xi = col(\xi_1, \cdots, \xi_N)$ with $\xi_i \in \mathbb{R}^n$ the element corresponding to the i^{th} vertex of $\mathcal{V}$, and $\bar{L} = I_n \otimes L$ with L the graph Laplacian of $\mathcal{G}$.

The GAS result for the DLKCF in observable modes is presented next.

Proposition 1 (Stability of the DLKCF for observable modes). *Consider the DLKCF in* (3.5) *and* (3.6) *with the consensus gain in* (3.7)–(3.8). *Suppose $Q_{i,k}$ is positive definite for all i and k, and all sections switch among the observable modes of the SMM. Then, the error dynamics of $\eta_{k|k}$ is GAS for sufficiently small γ_k, with consensus reached on the overlapping regions between neighbors.*

Proof. To conclude the GAS property of the error dynamics, we need to show $\delta V(k, \eta_{k|k})$ is negative when $\eta_{k|k} \neq 0$. To determine the sign of $\delta V(k, \eta_{k|k})$, we first analyse the signs of the three terms in (4.4) independently and then combine them together.

Step 1. Negative definiteness of the first term in δV

The proof for the first term follows closely from Lemma 3 in Olfati-Saber (2009), where the matrix inversion lemma is applied to show the negative definiteness of one-step change of the Lyapunov function candidate. Each element in the first term

in δV can be equivalently written as

$$\begin{aligned}
&\eta_{i,k|k}^T \left(A_{i,k}^T F_{i,k+1}^T \Gamma_{i,k+1|k+1}^{-1} F_{i,k+1} A_{i,k} - \Gamma_{i,k|k}^{-1} \right) \eta_{i,k|k} \\
=&\eta_{i,k|k}^T \left(A_{i,k}^T G_{i,k}^{-1} A_{i,k} - \Gamma_{i,k|k}^{-1} \right) \eta_{i,k|k} \\
=&-\eta_{i,k|k}^T \left(\Gamma_{i,k|k}^{-1} - A_{i,k}^T (A_{i,k} \Gamma_{i,k|k} A_{i,k}^T + W_k)^{-1} A_{i,k} \right) \eta_{i,k|k} \\
=&-\eta_{i,k|k}^T \Lambda_{i,k} \eta_{i,k|k},
\end{aligned}$$

where the first equation is obtained by $\Gamma_{i,k+1|k+1} = F_{i,k+1} G_{i,k+1} F_{i,k+1}^T$, and (recall that we assume $Q_{i,k} > 0$)

$$\begin{aligned}
W_k &= Q_{i,k} + \Gamma_{i,k+1|k} S_i \Gamma_{i,k+1|k} > 0 \\
\Lambda_{i,k} &= \Gamma_{i,k|k}^{-1} - A_{i,k}^T (A_{i,k} \Gamma_{i,k|k} A_{i,k}^T + W_k)^{-1} A_{i,k}
\end{aligned}$$

Multiplying $\Lambda_{i,k}$ from left and right by $\Gamma_{i,k|k}$ gives

$$\begin{aligned}
\Gamma_{i,k|k} \Lambda_{i,k} \Gamma_{i,k|k} &= \Gamma_{i,k|k} - \Gamma_{i,k|k} A_{i,k}^T (A_{i,k} \Gamma_{i,k|k} A_{i,k}^T + W_k)^{-1} A_{i,k} \Gamma_{i,k|k} \\
&= (\Gamma_{i,k|k}^{-1} + A_{i,k}^T W_k^{-1} A_{i,k})^{-1}
\end{aligned}$$

Multiplying the last equation from left and right by $\Gamma_{i,k|k}^{-1}$, we obtain

$$\Lambda_{i,k} = \Gamma_{i,k|k}^{-1} (\Gamma_{i,k|k}^{-1} + A_{i,k}^T W_k^{-1} A_{i,k})^{-1} \Gamma_{i,k|k}^{-1}$$

which is a symmetric and positive definite matrix. Thus the first term can be equivalently written as

$$\sum_{i=1}^{n} -\eta_{i,k|k}^T \Lambda_{i,k} \eta_{i,k|k} = -\eta_{k|k}^T \Lambda_k \eta_{k|k},$$

where $\Lambda_k = \mathrm{diag}(\Lambda_{1,k}, ..., \Lambda_{n,k})$, and we conclude the first term is negative definite.

Step 2. Negative semidefiniteness of the second term in δV

Using the quadratic property of the Laplacian in Lemma 2, we can render the second term of δV negative semidefinite by the consensus gain chosen in (3.7)–(3.8).

We introduce a new undirected graph $\hat{\mathcal{G}} = (\hat{\mathcal{V}}, \hat{\mathcal{E}})$ representing the topology of the overlapping regions with $\hat{\mathcal{V}}_k = \{\hat{\xi}_{\hat{i},k} : \hat{i} \in \hat{\mathcal{I}}\}$ for $\hat{\mathcal{I}} = \{1, \cdots, 2N-2\}$, and

$$\hat{\xi}_{\hat{i},k} = \begin{cases} \hat{I}_{i,j}\eta_{i,k|k-1} & \text{with } i = \frac{\hat{i}+1}{2},\ j = i+1, \text{ if } \hat{i} \text{ odd} \\ \hat{I}_{j,i}\eta_{j,k|k-1} & \text{with } i = \frac{\hat{i}}{2},\ j = i+1, \text{ if } \hat{i} \text{ even,} \end{cases}$$

$$\mathcal{N}_{\hat{i}} = \begin{cases} \{\hat{i}+1\} & \text{if } \hat{i} \text{ odd} \\ \{\hat{i}-1\} & \text{if } \hat{i} \text{ even.} \end{cases}$$

Suppose $n_{i,j} = \hat{n}$ for all $i \in \mathcal{I}$ and for all $j \in \mathcal{N}_i$, then $\hat{\xi}_{\hat{i},k} \in \mathbb{R}^{\hat{n}}$ for all $\hat{i}$. Let $\hat{L}$ be the $\hat{n}$ dimensional Laplacian of $\hat{\mathcal{G}}$. Denote $\hat{\xi}_k = \text{col}(\hat{\xi}_{1,k}, \cdots, \hat{\xi}_{2N-2,k}) = \hat{H}\eta_{k|k-1}$, where $\hat{H} = \text{Diag}(\hat{H}_1, \cdots, \hat{H}_n)$ with the i^{th} block on the diagonal

$$\hat{H}_i = \begin{cases} \hat{I}_{i,i+1} & \text{if } i = 1 \\ \hat{I}_{i,i-1} & \text{if } i = n \\ \begin{pmatrix} \hat{I}_{i,i-1}^T & \hat{I}_{i,i+1}^T \end{pmatrix}^T & \text{otherwise,} \end{cases}$$

and let $A_k = \text{diag}(A_{1,k}, \cdots, A_{N,k})$. Then by substituting the consensus gain (3.7) and the neighbor disagreement (4.1) into the second term of δV, and rewriting it in terms of the new graph $\hat{\mathcal{G}}$, we obtain:

$$\begin{aligned} &2\sum_{i=1}^{N}\left(\eta_{i,k+1|k}^T F_{i,k+1}^T \Gamma_{i,k+1|k+1}^{-1} \sum_{j\in\mathcal{N}_i} C_{i,k+1}^j u_{i,k+1}^j\right) \\ =&-2\gamma_k \eta_{k|k}^T A_k^T \hat{H}^T \hat{L} \hat{H} A_k \eta_{k|k} \leq 0. \end{aligned}$$

Thus it is concluded that the second term in δV is negative semidefinite.

Step 3. Positive definiteness of the third term in δV

Given the choice of consensus gain in (3.7)–(3.8), the third term in δV can be written as

$$\begin{aligned} &\sum_{i=1}^{N}\left(\sum_{j\in\mathcal{N}_i} C_{i,k+1}^j u_{i,k+1}^j\right)^T \Gamma_{i,k+1|k+1}^{-1} \left(\sum_{j\in\mathcal{N}_i} C_{i,k+1}^j u_{i,k+1}^j\right) \\ =&\gamma_k^2 \sum_{i=1}^{N}\left(\sum_{j\in\mathcal{N}_i} \hat{I}_{i,j}^T u_{i,k+1}^j\right)^T G_{i,k+1}^T \left(\sum_{j\in\mathcal{N}_i} \hat{I}_{i,j}^T u_{i,k+1}^j\right). \end{aligned}$$

We columnize $u_{i,k}^j$ over all neighbors $j \in \mathcal{N}_i$ within each section i and over all sections $i \in \mathcal{I}$, and denote it as u_k:

$$u_k = \mathrm{col}_{i\in\mathcal{I}}\left(\mathrm{col}_{j\in\mathcal{N}_i}\left(u_{i,k}^j\right)\right) = \tilde{L}\eta_{k|k-1} = \tilde{L}A_{k-1}\eta_{k-1|k-1},$$

where $\tilde{L}$ can be defined as a partitioned matrix with the $(\hat{i},i)^{\text{th}}$ block $\tilde{L}_{\hat{i},i}$ given by

$$\tilde{L}_{\hat{i},i} = \begin{cases} -\hat{I}_{i,i+1} & \text{if } \hat{i} \text{ is odd, and } i = \frac{1}{2}(\hat{i}+1) \\ \hat{I}_{i,i-1} & \text{if } \hat{i} \text{ is odd, and } i = \frac{1}{2}(\hat{i}+1)+1 \\ \hat{I}_{i,i+1} & \text{if } \hat{i} \text{ is even, and } i = \frac{\hat{i}}{2} \\ -\hat{I}_{i,i-1} & \text{if } \hat{i} \text{ is even, and } i = \frac{\hat{i}}{2}+1 \\ \mathbf{0} & \text{otherwise,} \end{cases}$$

where $\hat{i} \in \hat{\mathcal{I}}$ and $i \in \mathcal{I}$. Denoting $G_k = \mathrm{diag}(G_{1,k}, \cdots, G_{N,k})$, the third term in δV is equivalent to

$$\begin{aligned} &\gamma_k^2 \sum_{i=1}^{N} \left(\sum_{j\in\mathcal{N}_i} \hat{I}_{i,j}^T u_{i,k+1}^j\right)^T G_{i,k+1}^T \left(\sum_{j\in\mathcal{N}_i} \hat{I}_{i,j}^T u_{i,k+1}^j\right) \\ =&\gamma_k^2 \eta_{k|k}^T A_k^T \tilde{L}^T \hat{H} G_{k+1} \hat{H}^T \tilde{L} A_k \eta_{k|k} > 0, \end{aligned}$$

and it is positive definite since G_{k+1} is positive definite.

Step 4. The negative definiteness of $\delta V(k, \eta_{k|k})$

Provided Steps 1, 2, and 3, δV can be written as

$$\begin{aligned} \delta V(k,\eta_{k|k}) = &-\eta_{k|k}^T \left(\Lambda_k - \gamma_k^2 A_k^T \tilde{L}^T \hat{H} G_{k+1} \hat{H}^T \tilde{L} A_k\right) \eta_{k|k} \\ &- 2\gamma_k \eta_{k|k}^T A_k^T \hat{H}^T \hat{L} \hat{H} A_k \eta_{k|k}. \end{aligned}$$

Therefore by choosing γ_k sufficiently small we can render $\delta V(k, \eta_{k|k}) < 0$ for all $k \geq 0$ and for all $\eta_{k|k} \neq 0$. To be more precise, we need $\gamma_k < \gamma_k^*$ where γ_k^* is defined by

$$\gamma_k^* = \left(\frac{\lambda_{\min}\left(\Lambda_k\right)}{\lambda_{\max}\left(A_k^T \tilde{L}^T \hat{H} G_{k+1} \hat{H}^T \tilde{L} A_k\right)}\right)^{\frac{1}{2}}, \tag{4.5}$$

where $\lambda_{\min}$ and $\lambda_{\max}$ are the minimum and maximum eigenvalues of a matrix, respectively. Thus from Theorem 4.9 in Khalil (2002) we conclude that $\delta V(k, \eta_{k|k}) < 0$ for all $k \geq 0$ and for all $\eta_{k|k} \neq 0$, and therefore $\eta_{k|k} = 0$ is GAS for the error dynamics of the DLKCF. Consequently, all estimators reach a consensus on the overlapping regions between neighbors. □

Proposition 1 gives a formal analysis of the error dynamics of the DLKCF on a freeway segment where all the local sections switch among observable modes of the SMM (i.e., modes FF, CC, and CF), and shows its GAS property. This implies that the consensus term will not destabilize the filter, as long as the measurements available to each local agent are enough to reconstruct the traffic condition of its associated local region given the system model. In general, the KF is unstable under unobservable systems (see Burridge and Hall, 1987). Fortunately, the intrinsic property of the traffic model (i.e., the conservation of vehicles) serves as a crucial ingredient to stabilize the filter, and the next section explores the estimation error properties of the DLKCF under the unobservable modes of the SMM (i.e., modes FC1 and FC2).

4.2 Ultimate boundedness of estimate and property of estimation error in unobservable modes

Challenges for estimating the unobservable sections stem from the dependence of the system dynamics of the SMM on the state to be estimated (i.e. shock location and shock velocity), thus non-observability of the system will lead to unknown system dynamics. Moreover, with only upstream and downstream measurements, it can be shown that the unobservable modes are also undetectable.

In this section we first establish that the estimates of all the cells in an unobservable section are ultimately bounded inside $[-\varepsilon, \rho_m + \varepsilon]$ for all $\varepsilon > 0$, provided that

the upstream and downstream measurements are available. This property ensures that the estimates given by the DLKCF for unobservable modes are always physically meaningful to within ε. The conservation of the total error in the section (i.e. the sum of the estimation errors of all the cells in an unobservable section is constant) is proved in Morarescu and Canudas de Wit (2011) for a Luenberger observer when the output feedback is turned off in unobservable modes. In this section we prove a similar property in the KF framework accounting for the non-zero gain in the information update term.

4.2.1 Ultimate boundedness of the estimation error

First we present a lemma stating the boundedness of Kalman gain K_k, which is necessary for the boundedness of the estimates.

Lemma 3 (Boundedness of the Kalman gain for an undetectable system (Burridge and Hall, 1987))**.** *If the system* (3.1)-(3.2) *is undetectable, and all the undetectable modes are of unit modulus, then K_k is uniformly bounded from above for all $k \geq 0$.*

The *Kalman observability canonical form* of (2.5)-(2.6) shows that the eigenvalues of the observable subspace (i.e. the boundary cells) are one, and the unobservable subsystem has eigenvalues less than or equal to one (with the eigenvalue one corresponding to the shock location), which satisfies the assumptions of Lemma 3. We now establish the ultimate boundedness of the estimates, and for the remainder of Section 4.2 the section index i is dropped for notational simplicity.

Proposition 2 (Ultimate boundedness of the DLKCF for an unobservable section)**.** *Consider an unobservable section in a road network with dimension n. For all $\varepsilon > 0$, a finite time $T(\varepsilon)$ exists such that $\rho^l_{k|k} \in [-\varepsilon, \rho_m + \varepsilon]$ for all $k > T(\varepsilon)$ and for all $l \in \{1, \cdots, n\}$, independent of the initial estimate.*

Proof. The proof is by induction. For all $\varepsilon > 0$, since the upstream cell is in the observable subspace, we have $\rho^1_{k|k} \to \rho^1_k$, where $\rho^1_k \geq 0$. Hence a finite time $T_1(\varepsilon)$ exists such that $\rho^1_{k|k} > -\frac{\varepsilon}{n}$ for all $k > T_1(\varepsilon)$.

Suppose $\rho^{l-1}_{k|k} > -\frac{(l-1)\varepsilon}{n}$. For all $l \in \{2, \cdots, n\}$, if $\rho^l_{k|k} < -\frac{(l-1)\varepsilon}{n}$, we obtain from (2.4) that

$$q\left(\rho^{l-1}_{k|k}, \rho^l_{k|k}\right) = v_m \rho^{l-1}_{k|k} > -v_m \frac{(l-1)\varepsilon}{n}, \tag{4.6}$$

$$q\left(\rho^l_{k|k}, \rho^{l+1}_{k|k}\right) \leq v_m \rho^l_{k|k}. \tag{4.7}$$

Combining (4.6) and (4.7) with (2.3), and adding an information update term from the analysis step yields

$$\rho^l_{k+1|k+1} > \rho^l_{k|k} + \frac{v_m \Delta t}{\Delta x}\left|\rho^l_{k|k} + \frac{(l-1)\varepsilon}{n}\right| - c \parallel \eta^o_{k|k} \parallel_\infty, \tag{4.8}$$

where $c > 0$ is a finite scalar whose existence is guaranteed by the boundedness of Kalman gain, and we denote $\eta^o_{k|k} = \left(\eta^1_{k|k}, \eta^n_{k|k}\right)^T$ as the posterior estimation error of the upstream and downstream cells, which form an observable subspace, hence $\parallel \eta^o_{k|k} \parallel_\infty \to 0$ as $k \to \infty$. Thus from (4.8) we conclude that a class $\mathcal{K}^2$ function $\alpha(\cdot)$ and a continuous positive definite function $\mathcal{W}(|\cdot|)$ on $\mathbb{R}$ exist such that

$$\rho^l_{k+1|k+1} - \rho^l_{k|k} > \mathcal{W}\left(\left|\rho^l_{k|k} + \frac{(l-1)\varepsilon}{n}\right|\right),$$
$$\forall \left|\rho^l_{k|k} + \frac{(l-1)\varepsilon}{n}\right| \geq \alpha\left(\parallel \eta^o_{k|k} \parallel_\infty\right),$$

which indicates that the one-step change of the estimates is always positive, and the change rate is large enough so that a finite time $T_l(\varepsilon)$ exists such that $\rho^l_{k|k} > -\frac{l\varepsilon}{n}$ for all $k > T_l(\varepsilon)$ (see Khalil, 2002, Theorems 4.18 and 4.19). By induction we conclude that if $\rho^{n-1}_{k|k} > -\frac{(n-1)\varepsilon}{n}$, a finite time $T_n(\varepsilon)$ exists such that $\rho^n_{k|k} > -\varepsilon$ for all $k > T_n(\varepsilon)$. Letting $T(\varepsilon) = \max_l\{T_l(\varepsilon)\} = T_n(\varepsilon)$, we obtain $\rho^l_{k|k} > -\varepsilon$ for

[2]Recall that a continuous function $\alpha : [0, a) \to [0, \infty)$ is said to belong to class $\mathcal{K}$ if it is strictly increasing and $\alpha(0) = 0$.

all $k > T(\varepsilon)$ and $l \in \{1, 2, \cdots, n\}$. This proves the ultimate lower bound of the estimates.

The proof for an ultimate upper bound is similar, with a variation that the induction is conducted from n to 1. □

The essence of ultimate boundedness is that it rules out the possibility that the estimation error is destabilized in the analysis step, and the proof also shows the importance for having observable boundary states. Hence it is not ideal to drop the output feedback as in the Luenberger observer (Morarescu and Canudas de Wit, 2011), where the preservation of an ultimate bound $[-\varepsilon, \rho_m + \varepsilon]$ may fail due to the absence of output feedback loop and the pure reliance on the boundary conditions. This point is explored in more detail in Chapter 5.

4.2.2 Convergence of the sum of estimation errors across all the cells in an unobservable section

Despite the lack of ultimate boundedness, the advantage of an open-loop observer is that it ensures conservation of the sum of the estimation errors in an unobservable section. In this section we show that a similar property holds for the DLKCF under most conditions, and when it is not, it is sacrificed to preserve the ultimate boundedness of the estimates to within $[-\varepsilon, \rho_m + \varepsilon]$.

First we define three submodes in FC (i.e., FC1 $\bigcup$ FC2), which is important in specifying the condition under which the yet derived estimation error property holds. Note that the following definitions are applicable to both the true and the estimated state, and the submode for the true and the estimated state in an unobservable section may be different: (*i*) *Submode 1*, where the shock is located between cell $n-1$ and n, and has positive velocity (i.e. the section is about to switch from FC1 to FF); (*ii*) *Submode 2*, where the shock is located between cell 1 and 2, and has

negative velocity (i.e. the section is about to switch from FC2 to CC); and (*iii*) *Submode 3*, the state is neither in submode 1 nor in submode 2 (i.e. the section remains in FC1 or FC2).

We denote the sum of estimation errors across all the cells in an unobservable section as $Sum(\eta_{k|k}) = \sum_{l=1}^{n} \eta_{k|k}^{l}$. The property of estimation error we claim reads: *$Sum(\eta_{k|k})$ will converge to a fixed value (instead of being fixed as stated in an open-loop Luenberger observer), when both the true and the estimated states are in submode 3.* Under the specified condition, the flux between cell 1 and 2 is computed by the sending capacity of cell 1, and the flux between cell $n-1$ and n is computed by the receiving capacity of cell n.

Proposition 3 (Error property of the DLKCF for an unobservable section)**.** *Consider an unobservable section in a road network, and suppose both the true and the estimated states are in submode 3. Then $Sum(\eta_{k|k}) \to Sum(\eta)$ as $k \to \infty$.*

Proof. When the estimated and the true models may not match, the error dynamics is constructed as (recall that the consensus term is dropped in the unobservable mode)

$$\eta_{k+1|k+1} = F_k \left(\hat{A}_k \eta_{k|k} + \left(\hat{A}_k - A_k \right) \rho_k + \left(\hat{B}_k^{\rho} - B_k^{\rho} \right) \boldsymbol{\rho}_m \right), \tag{4.9}$$

where $\hat{A}_k$ is introduced in Remark 2. Define projection $P_1 : \mathbb{R}^{n \times n} \mapsto \mathbb{R}^{n-2 \times n-2}$ that cuts the first and last rows and columns of a matrix, and define projection $P_2 : \mathbb{R}^n \mapsto \mathbb{R}^{n-2}$ that cuts the first and last elements of a vector. When both the true and the estimated states are in submode 3, the estimated and true solutions of the boundary cells evolve with the same dynamics. Then applying P_2 to the left and right hand sides in (4.9) yields

$$\begin{aligned} P_2(\eta_{k+1|k+1}) = \; & P_1(\hat{A}_k) P_2(\eta_{k|k}) + \left(P_1(\hat{A}_k) - P_1(A_k) \right) P_2(\rho_k) \\ & + \left(P_1(\hat{B}_k^{\rho}) - P_1(B_k^{\rho}) \right) P_2(\boldsymbol{\rho}_m) + \epsilon_k, \end{aligned} \tag{4.10}$$

where $\epsilon_k = \left(\epsilon_k^2, \cdots, \epsilon_k^{n-1}\right)^T$, and

$$\epsilon_k^l = \begin{cases} \left(-k_{l,1} + \frac{v_m \Delta t}{\Delta x}\right) \eta_{k|k}^1 - k_{l,2} \eta_{k|k}^n & \text{if } l = 2 \\ -k_{l,1} \eta_{k|k}^1 + \left(\frac{w \Delta t}{\Delta x} - k_{l,2}\right) \eta_{k|k}^n & \text{if } l = n-1 \\ -k_{l,1} \eta_{k|k}^1 - k_{l,2} \eta_{k|k}^n & \text{otherwise,} \end{cases}$$

with $k_{i,j}$ representing the $(i,j)^{\text{th}}$ entry of K_{k+1}. Adding all the state variables of the left and right hand sides of (4.10) yields

$$\begin{aligned} \textstyle\sum_{l=2}^{n-1} (\eta_{k+1|k+1}^l) = \; & \textstyle\sum_{l=2}^{n-1} (\eta_{k|k}^l) - \sum_{l=2}^{n-1} \left(k_{l,1} \eta_{k|k}^1 + k_{l,2} \eta_{k|k}^n\right) \\ & + \tfrac{v_m \Delta t}{\Delta x} \eta_{k|k}^1 + \tfrac{w \Delta t}{\Delta x} \eta_{k|k}^n, \end{aligned} \tag{4.11}$$

where the first term of the right hand side in (4.11) is derived in Morarescu and Canudas de Wit (2011), and the remaining terms are derived by direct calculation. Note that $\eta_{k|k}^1$ and $\eta_{k|k}^n$ are the estimation errors of the observable subspace with linear time-invariant dynamics and (uniformly) complete observability, so they decay exponentially fast (see Jazwinski, 1970, Theorems 7.4 and 7.5). Moreover, the Kalman gain K_k is bounded, hence $\sum_{l=2}^{n-1} (\eta_{k|k}^l)$ converges, and consequently $Sum(\eta_{k|k})$ converges. □

Admittedly, there is no guarantee that the submode assumption in Proposition 3 will always hold. Even worse, eventually it should fail unless the queue never grows outside the section or never dissipates. However, by examining the cases when the assumption fails we find some nice properties of the DLKCF. Consider the case when the estimated state is in submode 2, but the true state is in submode 3. If we insist on conserving the sum of the errors, the vehicles in the upstream cells will eventually be over-saturated (resulting in estimates larger than ρ_m). While in the DLKCF, the estimated inflow of each cell is computed based on its receiving capacity, thus no cell is forced to accept vehicles beyond its capacity to ensure error conservation. We will show experimental results for this in Chapter 5.

Chapter 5

Numerical experiments

In this chapter, we assess the performance of the DLKCF under different scenarios. We first show the estimation results of the DLKCF for a *Riemann problem* (LeVeque, 2002), and validate the GAS of error dynamics under observable modes when properly accounting for the modeling errors on the boundaries. Then under a more complex experiment, we show that in unobservable sections the estimates given by the DLKCF are ultimately bounded inside $[-\varepsilon, \rho_m + \varepsilon]$, while the estimates of a Luenberger observer may take physically unreasonable values. We also illustrate the relationship between the sum of the errors and the submodes of the true and the estimated states. Next we evaluate the DLKCF by comparing it with the performance when dropping the consensus term and individual local KFs without inter-agent communication, and show that the DLKCF has less disagreement on estimates among neighbors, less overall estimation error, and more robustness to low quality sensors or agents. Finally we close our discussion by analysing the computational complexity of the DLKCF, and show a considerable reduction of its runtime per agent compared to a central KF to perform the same estimation task.

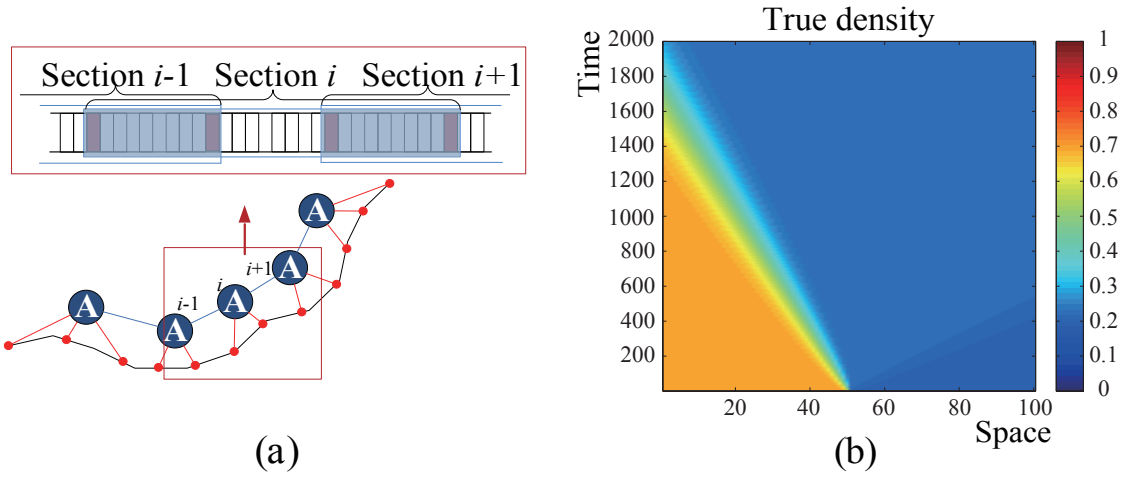

Figure 5.1: The network and true solution setup of the experiment to estimate an expansion fan.

a) Freeway network setup and the communication topology between estimation agents (capital A in circles) and sensors (red dots), with blue lines standing for connections between agents, and red lines representing connections between agent and sensors. The network is simplified into a one-dimensional straight line, discretized by cells (small rectangles) and localized by sections (blocks). Sensor locations are represented by red cells; b) True solution of a Riemann problem (expansion fan).

5.1 GAS under Observable Modes

We first present an experiment where the initial condition of the entire network is piecewise constant, and the true solution is approximated using the Godunov scheme (2.3). We show that the negative effect of assigning constant boundary dynamics in our SMM can be attenuated by imposing larger modeling errors on the corresponding boundaries.

The network setup and the communication topology is illustrated in Fig. 5.1a. The network is a stretch of highway divided into 100 cells and 5 sections. For the DLKCF, each section has 28 cells, with the left and right 10 cells overlapping with its left and right neighbors, respectively.

We apply normalized parameters for the triangular fundamental diagram, and

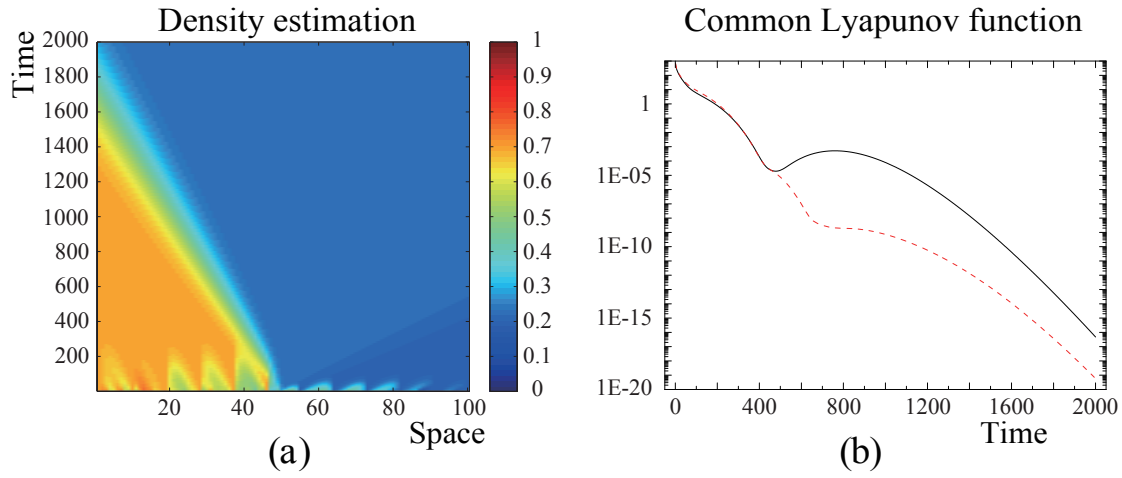

Figure 5.2: Estimation of an expansion fan.

a) State estimates by the DLKCF; b) Evolution of the common Lyapunov function without (solid line) and with (dashed line) increases on the standard deviations of model noise on the boundary cells.

analyse the behaviour of the DLKCF when the true solution is an expansion fan (see Fig. 5.1b). Parameter not detailed here (same for the remainder of the numerical experiments) can be found in the README documentation for the supplementary source code (Sun and Work, 2014).

The estimation of the expansion fan given by the DLKCF is illustrated in Fig. 5.2a. Note that in order to validate the GAS of estimation error, measurement noise is turned off for this experiment to check the convergence of the estimation error (in mean) to zero. The evolution of the common Lyapunov function (4.3) is plotted in Fig. 5.2b, with the solid line denoting the common Lyapunov function for the estimate in Fig. 5.2a, and with the dashed line denoting an estimate when the standard deviation of model noise is increased to 0.3 at the boundary cells with constant dynamics (compared to 0.03 at the interior cells). It is shown that by increasing the standard deviation of model noise on the boundary we yield a monotonically decreasing common Lyapunov function.

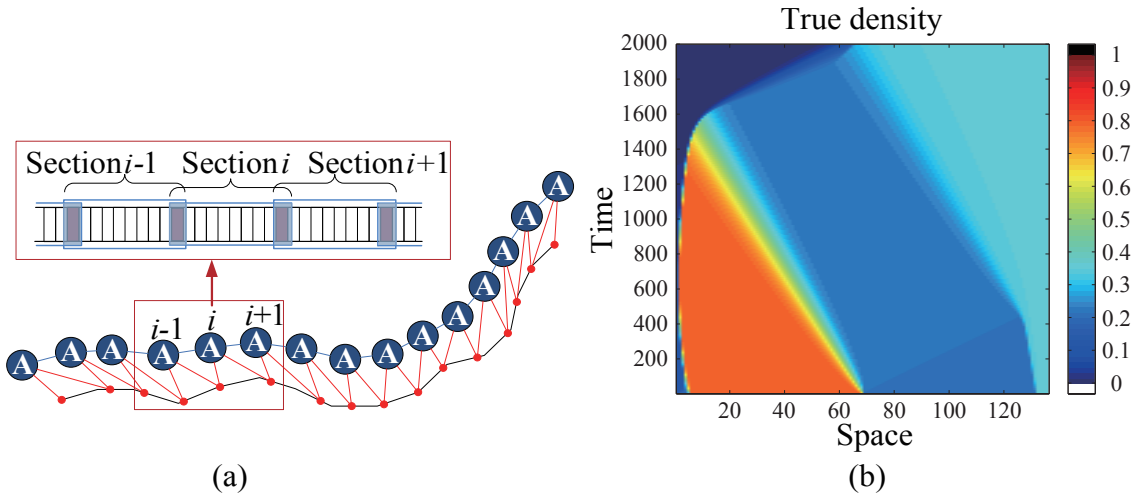

Figure 5.3: The network and true solution setup to compare the ultimate boundedness and the error property of the estimates given by the DLKCF and a Luenberger observer.

(a) Freeway network setup and communication topology for the DLKCF (in this setup the sensor locations coincide with the shaded overlapping regions); (b) True solution set to be a combination of an expansion fan and a shock propagating upstream, with a sinusoidal upstream boundary condition.

5.2 Ultimate bound and error property

In this section, we compare the performance of the DLKCF and a Luenberger observer (Sun et al., 2003; Morarescu and Canudas de Wit, 2011) to illustrate the discussions in Section 4.2. The network setup and the communication topology for the DLKCF is shown in Fig. 5.3a. The network is a stretch of highway divided into 136 cells and 15 sections. Both the DLKCF and the Luenberger observer have 10 cells in each section, with the left and right boundary cells overlapping with its left and right neighbors, respectively. The true solution is set to be a combination of an expansion fan and a shock propagating upstream, with a sinusoidal upstream boundary condition (Fig. 5.3b).

The estimates given by the DLKCF and the Luenberger observer are illustrated in Fig. 5.4, where the black and white areas depict estimates that are larger than

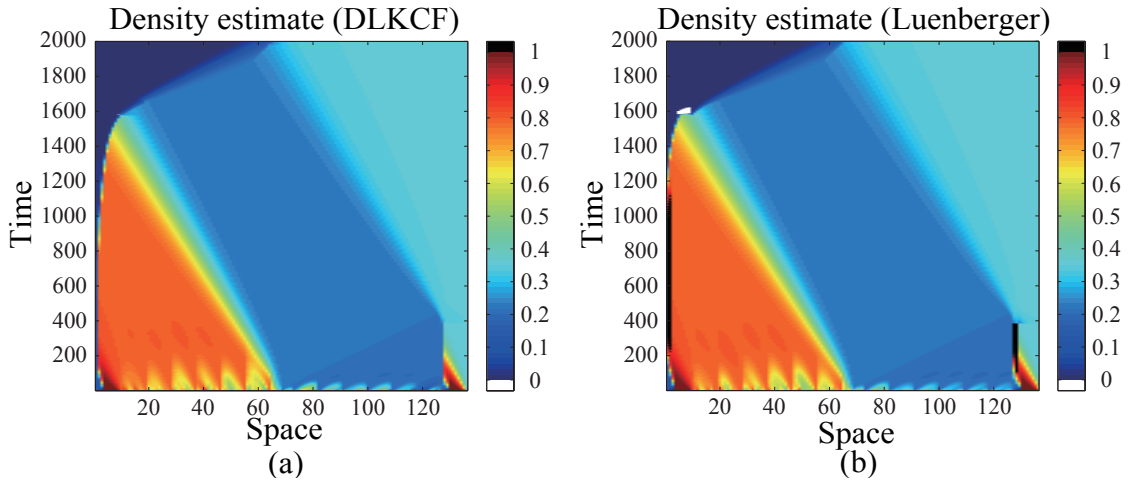

Figure 5.4: Comparison of the state estimates given by the DLKCF and a Luenberger observer.

(a) State estimates given by the DLKCF; (b) State estimates given by a Luenberger observer. The black areas represent estimates greater than the jam density, and the white areas represent estimates smaller than zero.

ρ_m and less than zero, respectively. Note that to rule out the possibility that the nonphysical estimates are caused by a randomly generated large measurement error, and to validate the expected estimation error property, measurement noise is turned off for this experiment. The black area (see Fig. 5.4b) appears because the estimated shock propagates to the upstream boundary before the true shock, and the estimator is forced to accept an inflow greater than the receiving capacity of its upstream boundary cell. Nevertheless, if the boundary conditions are sufficiently accurate, and a warm-up period is introduced to eliminate the estimation error when the section first arrives at a FC mode, then the chance a Luenberger observer could suffer from this can be considerably reduced. The white area is generated in the FF mode by the refinement in the analysis step, which is relatively large since the section has been unobservable for a long period of time.

Fig. 5.5 presents the relationship between the sum of the estimation errors and the submodes in section 0 and 14, where the estimates given by the Luenberger

observer occasionally show nonphysical values. It is illustrated that when the section is in FC, the sum of error provided by the Luenberger observer is always fixed, while it is more flexible for the DLKCF. When the estimated state is in submode 2 but the true solution remains in submode 3, the DLKCF will drop vehicles at the upstream boundary, thus resulting in a decrease in the sum of the estimation errors, and the decrease stops when the true state finally arrives in submode 2. The case is similar when the DLKCF needs to add more vehicles at the downstream boundary to avoid estimates of negative densities. Finally note that by truncating the nonphysical estimates to within the desired bound, the Luenberger observer can also achieve reasonable estimates at the expense of error conservation, which is similar to the case of the DLKCF where the error property proved in Section is sacrificed to preserve ultimate boundedness of the estimates.

5.3 Effect of inter-agent communication

In this section, we show the effect of the distributed algorithm on producing accurate estimates, and the critical role the consensus term plays in reducing the disagreement between agents. The network setup is given in Fig. 5.6, with the true solution being the same as in Section 5.2 (see Fig. 5.3b).

Disagreement and estimation errors can be generated for various reasons, and in this experiment we consider the combining effects of the following two causes: (i) *low quality sensors*, with some of the sensors having large measurement errors; (ii) *low quality agents*, with some agents assuming incorrect (too small) noise models for the low quality sensors.

Table 5.1 explores the effects of the above two causes on the disagreement and error of estimates for individual local KFs, the *Distributed Local Kalman Filter* (DLKF) which denotes the DLKCF without a consensus term, and the DLKCF.

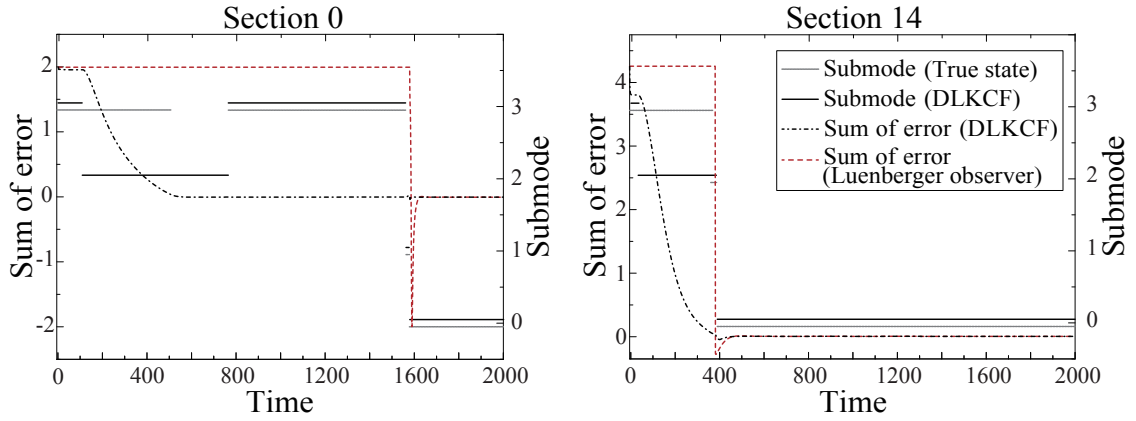

Figure 5.5: The relationship between the sum of the errors across an unobservable section and its submodes.

The sum of the errors for the DLKCF and the Luenberger observer (left axis), and the submodes of the true state and the estimated state given by the DLKCF (right axis). The index 0 on the right axis means that the section is in one of the observable modes, and 1, 2, 3 correspond to the unobservable submodes 1, 2, and 3 defined in Section 5.2. To better distinguish between the submode plots for the true state and the estimated state given by the DLKCF, the submode indices are slightly perturbed by -0.05 and 0.05, respectively. The submode plot for the estimated state given by the Luenberger observer is not shown here since the sum of the errors is always constant as long as the section is unobservable, independent of the submode.

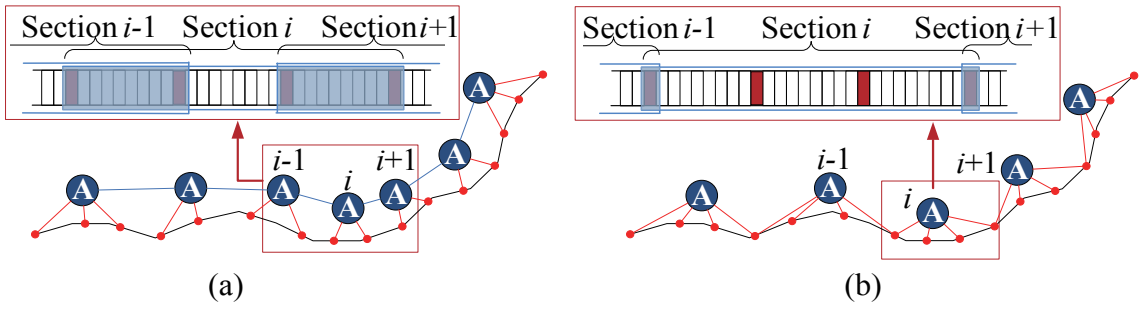

Figure 5.6: The network setup to validate the effect of inter-agent communication. (a) Freeway network setup and communication topology for the DLKCF; (b) Freeway network setup and communication topology for the individual local KFs.

Table 5.1: Disagreement and error of estimate[1]

Low quality		Disagreement ($\times 10^{-1}$)			Error ($\times 10^{-1}$)		
sensors	agents	Idv. KF	DLKF	DLKCF	Idv. KF	DLKF	DLKCF
False	–	0.014	0.585	0.354	1.133	1.133	1.106
True	False	0.148	0.558	0.310	1.461	1.470	1.453
True	True	1.631	1.648	1.085	2.856	1.555	1.531

[1] Idv. is the abbreviation for individual.

Starting from the downstream sensor of the first section, we put a low quality sensor (with the measurement error standard deviation of 0.3, compared to 0.03 for all other sensors) once every three sensors, and we assume that agents indexed by even numbers cannot recognize the low quality sensors they are connected to (thus still applying 0.03 as the measurement error standard deviation for the low quality sensors). We also apply perturbations of 10-20 percent on the parameters in the traffic model (i.e. ρ_m, ρ_c, and v_m) in the estimators for different agents. The disagreement u of the estimate is computed by $u = \left(\frac{1}{k_{\max}} \sum_{k=1}^{k_{\max}} u_k\right)^{\frac{1}{2}}$, where $k_{\max}$ is the total number of time steps, and $u_k = \frac{1}{N-1} \sum_{i=1}^{N-1} \frac{\|u_{i,k}^{i+1}\|_2^2}{n_{i,i+1}}$ with $u_{i,k}^{i+1}$ defined in (4.1). The average estimation error is given by $\eta = \left(\frac{1}{k_{\max}} \sum_{k=1}^{k_{\max}} \eta_k\right)^{\frac{1}{2}}$, where $\eta_k = \frac{1}{N} \sum_{i=1}^{N} \frac{\|\eta_{i,k|k}\|_2^2}{n_i}$.

Table 5.1 indicates the sensitivity of individual local KFs to the existence of low quality sensors and agents, with the disagreement and error considerably increasing as low quality sensing and estimating units are added in the system, and Fig. 5.7 plots the corresponding estimates given by the individual local KFs and the DLKCF. The sensors and the low quality agents for the two estimators are identical. However, for individual local KFs the low performance agents can never identify the low quality sensors they are connected to, while in the DLKCF some of the low performance agents apply the right measurement error covariance matrices through communication with neighbors. Consequently, it is shown in Fig. 5.7a that the estimates given by the independent low performance agents with low quality sensors

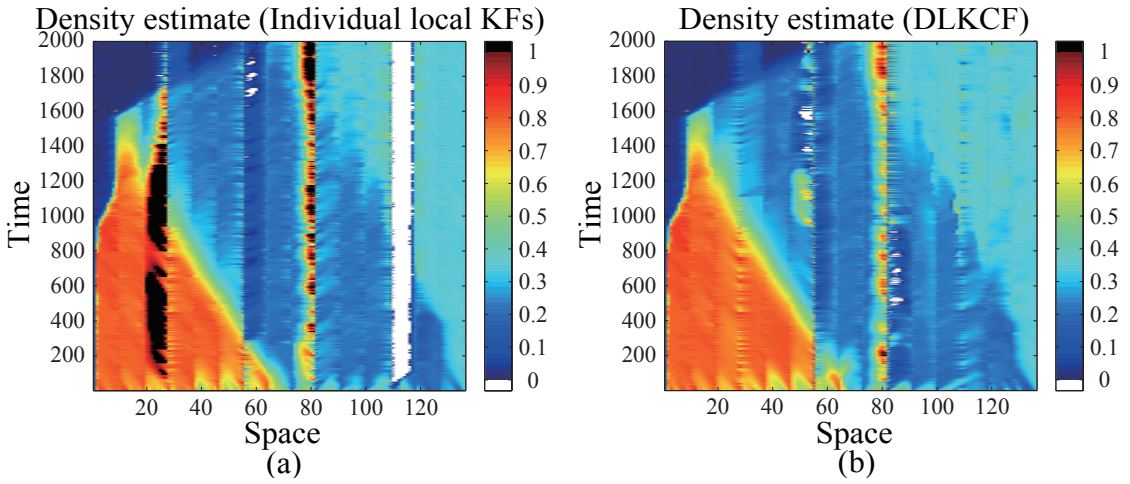

Figure 5.7: Estimation with low quality sensors and agents.
(a) State estimates given by individual local KFs; (b) State estimates given by the DLKCF.

are poor. Comparatively, the estimates given by the DLKCF is much better due to the strong connection among agents through overlapping regions and inter-agent communications (see also Fig. 5.6a).

Fig. 5.8 illustrates the evolution of disagreements u_k and errors η_k for the individual local KFs, the DLKF, and the DLKCF. It is shown that the disagreement and error for individual local KFs is large and fluctuates compared to the DLKF and DLKCF. Fig. 5.8b illustrates that the DLKF is significant in reducing the estimation error. Notice that at some time periods the disagreement of the DLKCF may increase to the level comparable to the individual local KFs, since it is not guaranteed that all the low quality sensors can be identified through inter-agent communication. Despite this, it is shown that the disagreement of the DLKF is reduced through the consensus term in the DLKCF. In general, the effect of the consensus term is more apparent if the disagreement before applying a consensus term is relatively large.

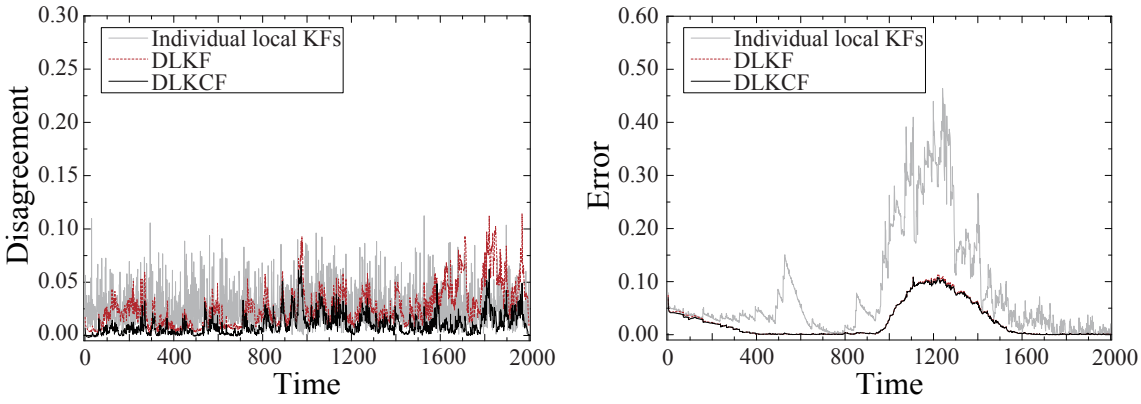

Figure 5.8: Disagreement and error for the DLKCF, the DLKF, and individual local KFs.

5.4 Computational complexity

In this section, we close the loop by returning to the point that motivates this work– reducing the computational load of the estimators. We analyse the computational complexity of the DLKCF, and compare its runtime with a central KF where a central estimator estimates the entire network.

Recall that the multiplication of two matrices in $\mathbb{R}^{n\times n}$ is regarded as an $O(n^3)$ operation, and the multiplication of a matrix in $\mathbb{R}^{n\times n}$ and a vector in $\mathbb{R}^n$ is an $O(n^2)$ operation. Thus a standard KF with state in $\mathbb{R}^n$ has an $O(n^3)$ computational complexity at each estimation step.

For the i^{th} local agent of the DLKCF, the computational complexity of conducting the forecast step, as well as updating the posterior error covariance in the analysis step, is $O(n_i^3)$ at each estimation step. As for computing the posterior estimate, the computational complexity is dominated by the required operations to obtain the consensus term (i.e., to compute the γ_k^*). Recall from (4.5) that the value of γ_k^* is obtained by computing the minimum and maximum eigenvalues of particular matrices whose dimensions are closely related to the structure of the network. For

Table 5.2: Runtime comparison of the central KF and the DLKCF (per agent) to complete 2000 estimation steps

Central KF		DLKCF			
n	runtime t_c (sec)	n	n_l	$\hat{n}$	runtime t_d (sec)
100	104	100	28	10	19.4
210	512	210	50	10	68.6
460	4400	460	100	10	336

simplicity we assume $n_i = n_l$ for all i, where the subscript "l" stands for "local", then we have $A_k, G_k \in \mathbb{R}^{Nn_l \times Nn_l}$, and $\tilde{L}, \hat{H} \in \mathbb{R}^{2(N-1)\hat{n} \times Nn_l}$ (recall that $\hat{n}$ is the dimension of the overlapping areas). If we apply eigenvalue searching methods which are able to ensure rapid convergence within a few iterations (e.g., the *Rayleigh Quotient Iteration* (see Heath, 2002, Section 4.3), etc.), obtaining the consensus term requires an $O(N^3 n_l^2 \hat{n})$ operation. Thus the computational complexity of the DLKCF for the i^{th} local agent is dominated by $O(N^3 n_i^2 \hat{n} + n_i^3)$ at each estimation step, and here we apply the subscript i back for consistency[1]. Note that the sparsity of the matrices A_k, $\tilde{L}$ and $\hat{H}$, which will potentially reduce the computational load, is not considered in this analysis.

Table 5.2 reports the runtime for each agent of the DLKCF and the central KF to complete 2000 estimation steps tracking a shockwave on a stretch of freeway, which we denote as t_d and t_c, respectively. The state dimensions n for the DLKCF and the central KF are the same. For the DLKCF, the number of local sections N and the number of overlapping cells between neighbors $\hat{n}$ remain unchanged as n increases, and we let $n_i = n_l$ for all i. It is shown in Table 5.2 that compared to the central KF, the runtime of the DLKCF is considerably reduced, and $t_d \approx t_c^{\frac{2}{3}}$. This is due to the fact that if we let $n \approx Nn_l$, then at each estimation step the central KF requires $O(N^3 n_l^3)$ operations, and the required operations for the DLKCF per agent

[1]If we further assume that $N \ll n_l$ (i.e., the total number of the local sections is much smaller than the dimension of the local sections), the computational complexity of the DLKCF for the i^{th} local agent is dominated by $O(n_i^2 \hat{n} + n_i^3)$.

is approximately $O(N^3 n_l^2 \hat{n})$, assuming the complexity for computing the consensus term dominates the local KF. Further if we consider $N \ll n_l$ and $\hat{n} \ll n_l$, and the sparsity of the matrices A_k, $\tilde{L}$ and $\hat{H}$ encountered in the computation of the consensus term, we obtain $O(N^3 n_l^2 \hat{n}) \approx O(N^2 n_l^2)$, which yields $t_d \approx t_c^{\frac{2}{3}}$.

Chapter 6

Conclusions and future work

In this work, a distributed local Kalman consensus filter is designed, analysed and validated for large-scale multi-agent traffic estimation. The DLKCF is applied to the switching mode model to monitor traffic on a road network partitioned into local sections, with overlapping regions between neighbors introduced to allow for information exchange on measurements and estimates. We prove that the error dynamics of the DLKCF is globally asymptotically stable when all sections switch among observable modes of the SMM. For an unobservable section, we show that the estimates are ultimately bounded, thus ensuring physically meaningful estimates. We also prove that under most conditions, the sum of the estimation errors of all the cells in the unobservable section converges to a fixed value. Numerical experiments verify the GAS of the error dynamics under observable modes, compare the DLKCF to a Luenberger observer when unobservable sections exist, illustrate the effect of the DLKCF on promoting agreement among different agents as well as reducing the overall estimation error, and shows a considerable reduction on the runtime of the DLKCF compared to a central KF.

Several other related problems are open for future exploration. Currently, the scaling factor γ_k in the consensus term is globally shared among all the local sections, indicating that the computation of γ_k requires incorporating the structure of the entire road network, which is computationally expensive. The DLKCF will be

significantly improved if scaling factors $\gamma_{i,k}$ can be locally obtained based only on the structure of the i^{th} section and its neighbors.

In this work, the consensus term is turned off in the unobservable section, since we do not want them to attempt to correct their neighbors when their own estimates are poor, and since the ultimate boundedness of the estimates is shown to exist without the consensus term. It would be interesting to see if we can find consensus structures that can help the unobservable sections achieve better estimates by communicating with observable neighbors, while preserving the stability or boundedness of the estimation error.

Another potential future work is to assess the DLKCF in a field experiment. One of the major challenges is to generalize all the results to the case where junctions exist to link several stretches of roadways. Despite this, undoubtedly it would be worth either deriving the network extension and doing a field assessment, and possibly comparing with other filters.

Bibliography

S. Blandin, A. Couque, A. Bayen, and D. B. Work. On sequential data assimilation for scalar macroscopic traffic flow models. *Physica D: Nonlinear Phenomena*, 241 (17):1421–1440, 2012.

G. Boker and J. Lunze. Stability and performance of switching Kalman filters. *International Journal of Control*, 75(16-17):1269–1281, 2002.

P. Burridge and A. Hall. Convergence of the Kalman filter gain for a class of non-detectable signal extraction problems. *IEEE Transactions on Automatic Control*, 32(11):1036–1039, 1987.

C. Canudas de Wit, L. R. Leon Ojeda, and A. Kibangou. Graph constrained-CTM observer design for the Grenoble south ring. *13th IFAC Symposium on Control in Transportation Systems*, 2012.

H. Chen and H. A. Rakha. Prediction of dynamic freeway travel times based on vehicle trajectory construction. In *Proceedings of the 15th IEEE Conference on Intelligent Transportation Systems*, pages 576–581, 2012. doi: 10.1109/ITSC.2012.6338825.

C. F. Daganzo. The cell transmission model: a dynamic representation of highway traffic consistent with the hydrodynamic theory. *Transportation Research Part B: Methodological*, 28(4):269–287, 1994.

C. F. Daganzo. The cell transmission model, part II: network traffic. *Transportation Research Part B: Methodological*, 29(2):79–93, 1995.

A. Fax and R. M. Murray. Information flow and cooperative control of vehicle formations. *IEEE Transactions on Automatic Control*, 49(9):1465–1476, 2004.

C. Godsil and G. Royle. *Algebraic graph theory*. Springer, 2001.

S. Godunov. A difference method for the numerical calculation of discontinuous solutions of hydrodynamic equations. *Mathematics Sbornik*, 47(3):271–306, 1959.

M. T. Heath. *Scientific computing: An introductory servey*. McGraw-Hill, INC., 2nd edition, 2002.

S. Jabari and H. Liu. A stochastic model of traffic flow: theoretical foundations. *Transportation Research Part B: Methodological*, 46(1):156–174, 2012.

S. Jabari and H. Liu. A stochastic model of traffic flow: Gaussian approximation and estimation. *Transportation Research Part B: Methodological*, 47:15–41, 2013.

A. H. Jazwinski. *Stochastic process and filtering theory*. Academic Press, 1970.

H. Khalil. *Nonlinear systems*. Prentice Hall, 3rd edition, 2002.

U. A. Khan and J. M. F. Moura. Distributing the Kalman filter for large-scale systems. *IEEE Transactions on Signal Processing*, 56(10):4919–4935, 2008.

J. P. Lebacque. The Godunov scheme and what it means for first order traffic flow models. In *Proceedings of the 13th International Symposium on Transportation and Traffic Theory*, pages 647–677, 1996.

R. LeVeque. *Finite volume methods for hyperbolic problems*. Cambridge University Press, 2002.

M. Lighthill and G. Whitham. On kinematic waves. II. A theory of traffic flow on long crowded roads. *Proceedings of the Royal Society of London. Series A, Mathematical and Physical Sciences*, 229(1178):317–345, 1955.

N. Lynch. *Distributed algorithms*. Morgan Kaufmann Publishers, 1997.

M. Mesbahi and M. Egerstedt. *Graph theoretic methods in multiagent networks*. Princeton University Press, 2010.

L. Mihaylova, R. Boel, and A. Hegyi. Freeway traffic estimation within recursive Bayesian framework. *Automatica*, 43(2):290–300, 2007.

L. Mihaylova, A. Hegyi, A. Gning, and R. Boel. Parallelized particle and Gaussian sum particle filters for large-scale freeway traffic systems. *IEEE Transactions on Intelligent Transportation Systems*, 13(1):36 – 48, 2012.

I. Morarescu and C. Canudas de Wit. Highway traffic model-based density estimation. In *Proceedings of the American Control Conference*, volume 3, pages 2012–2017, 2011.

F. Morbidi, L. L. Ojeda, C. Canudas de Wit, and I. Bellicot. A new robust approach for highway traffic density estimation. In *Proceedings of the 13th European Control Conference*, pages 1–6, 2014.

L. Munoz, X. Sun, R. Horowitz, and L. Alvarez. Piecewise-linearized cell transmission model and parameter calibration methodology. *Transportation Research Record*, (1965):183–191, 2006.

R. Olfati-Saber. Distributed Kalman filter with embedded consensus filters. In *Proceedings of the 44th IEEE Conference on Decision and Control, and European Control Conference*, pages 8179–8184, 2005.

R. Olfati-Saber. Distributed Kalman filtering for sensor networks. In *Proceedings of the 46th IEEE Conference on Decision and Control*, pages 5492–5498, 2007.

R. Olfati-Saber. Kalman-consensus filter: optimality, stability, and performance. In *Proceedings of the 48th IEEE Conference on Decision and Control*, pages 7036–7042, 2009.

R. Olfati-Saber, A. Fax, and R. Murry. Consensus and cooperation in networked multi-agent systems. *Proceedings of the IEEE*, 95(1):215–233, 2007.

H. Payne. Models of freeway traffic and control. *Simulation Council Proceedings*, 1: 51–61, 1971.

B. S. Y. Rao, H. F. Durrant-Whyte, and J. A. Scheen. A fully dencentralized multi-sensor system for tracking and surveillance. *International Journal of Robotics Research*, 12(1):20–44, 1993.

P. I. Richards. Shock waves on the highway. *Operations Research*, 4(1):42–51, 1956.

N. Santoro. *Design and analysis of distributed algorithms*. Wiley-Interscience, 2007.

J. L. Speyer. Computation and transmission requirements for a decentralized linear-quadratic-Gaussiaon control problem. *IEEE Transactions on Automatic Control*, 24(2):266–269, 1979.

X. Sun, L. Munoz, and R. Horowitz. Highway traffic state estimation using improved mixture Kalman filters for effective ramp metering control. In *Proceedings of the 42nd IEEE Conference on Decision and Control*, pages 6333–6338, 2003.

X. Sun, L. Munoz, and R. Horowitz. Mixture Kalman filter based highway congestion mode and vehicle density estimator and its application. In *Proceedings of the American Control Conference*, pages 2098 – 2103, 2004.

Y. Sun and D. B. Work. Source code for the distributed local Kalman consensus filter (MS thesis), 2014. URL `https://github.com/yesun/DLKCFthesis`.

J. Thai and A. Bayen. State estimation for polyhedral hybrid systems and applications to the Godunov scheme. In *Proceedings of the 16th International Conference on Hybrid Systems: Computation and Control*, pages 143–152, 2013.

Y. Wang and M. Papageorgiou. Real-time freeway traffic state estimation based on extended Kalman filter: a general approach. *Transportation Research Part B: Methodological*, 39(2):141–167, 2005.

G. Whitham. *Linear and nonlinear waves*. John Wiley & Sons, Inc., New York, NY, 1974.

D. B. Work, S. Blandin, O.-P. Tossavainen, B. Piccoli, and A. Bayen. A traffic model for velocity data assimilation. *Applied Mathematics Research eXpress*, 2010(1): 1–35, 2010. doi: 10.1093/amrx/abq002.

Y. Yuan, J. van Lint, R. Wilson, F. van Wageningen-Kessels, and S. Hoogendoorn. Real-time Lagrangian traffic state estimator for freeways. *IEEE Transactions on Intelligent Transportation Systems*, 13(1):59–70, 2012.